Exploratory FEM-Based Multiphysics Oxygen Transport and Cell Viability Models for Isolated Pancreatic Islets

Peter Buchwald*
Diabetes Research Institute and the Department of Molecular and Cellular Pharmacology, University of Miami, Miller School of Medicine
*Corresponding author: DRI, 1450 NW 10th Ave (R-134), Miami, FL 33136, USA; pbuchwald@med.miami.edu

Abstract: Exploratory cellular-level oxygen consumption and cell viability models incorporating physiologically realistic assumptions and fully scaled 2D/3D geometries have been implemented in COMSOL Multiphysics for isolated pancreatic islets. Such models are of considerable interest to improve the function and viability of cultured, transplanted, or encapsulated islets. Oxygen consumption was assumed to follow Michaelis-Menten–type kinetics and to cease when local concentrations fell below a critical threshold. By introducing this consumption-rate into the standard system of differential equations describing convective and diffusive transport, $\partial c/\partial t+\nabla\cdot(-D\nabla c)=R-\mathbf{u}\cdot\nabla c$, realistic quantitative models could be obtained. Results are in good agreement with experimental observations suggesting frequent hypoxia-related cell death (necrosis) in the core regions of larger islets. Furthermore, by coupling this convection and diffusion model to COMSOL's incompressible Navier–Stokes fluid-mechanics and other application modes, true multiphysics models could be obtained for more complex cases such as perifusion chambers with flowing media or culture plates with rocking plate-induced agitation.
Keywords: Islets of Langerhans, oxygen consumption, cell culture, diabetes mellitus.

1. Introduction

Type 1 (insulin-dependent or juvenile-onset) diabetes mellitus results from the autoimmune destruction of the insulin-producing pancreatic β-cells and requires continuous glucose monitoring and insulin treatment. Chronic and degenerative complications still occur in a considerable fraction of patients. Transplantation of pancreatic islet cells is being explored as an experimental therapy for a selected cohort of patients, and, in the US, is currently conducted under an IND (Investigational New Drug) application at several centers. It can normalize metabolic control in a way that has been virtually impossible to achieve with exogenous insulin, but because of the life-long immunosuppression required, the procedure is currently limited to the most severe forms of diabetes [1]. Nevertheless, results are improving continuously [1] mainly due to improved islet preparation techniques and the availability of more effective immuno-suppressive regimens such as those of the so-called Edmonton protocol [2]. Currently, as a standard practice, islets are cultured for up to two days before being transplanted because this allows the islets to recover from the isolation-induced damage and also makes possible the recipient's travel to the transplantation site, the start of the immunosuppression before transplantation, and the assessment of the quality and safety of the islets. However, the survival and functionality of these islets that lost their vasculature during the isolation process and have to rely on passive diffusion is often seriously affected by hypoxia during culture or immediately following transplantation. Hence, the spatio-temporal modeling of oxygen consumption of pancreatic islets (and of other tissues) is an important general goal in itself, but it is of particular interest for the development of improved cell culture and bioartificial pancreas-type devices (with encapsulated or non-encapsulated islets).

Pancreatic islets are structurally well-defined spheroidal cell aggregates of about 1,500–2,000 cells and diameters of about 150 μm (range: 50–500 μm) that contain the endocrine cells of the pancreas (α, β, γ, and PP-cells), whose main role is to secrete hormones that regulate blood glucose levels. They have an extensive intra-islet vasculature [3-5], which is essential to supply oxygen and nutrients and to remove metabolic waste products, especially for the inner core. Islets have a very high blood perfusion, similar to that of the renal cortex (i.e., 5–7 $mL\cdot min^{-1}g^{-1}$), and while they constitute only about 1–2% of the pancreas by weight, they receive around 10–20% of the total blood flow of the pancreas [6-8].

During islet isolation and culture, this vasculature gets disrupted so that islets are initially avascular after transplantation, and perfusion of the core is compromised. Hence, cultured or encapsulated (immune-isolated) islets, as well as all transplanted islets during the initial few days of transplantation have to depend on the passive diffusion of oxygen and nutrients from the periphery, which limits the oxygen and nutrient supply in the inner core of islets, especially larger islets, and can ultimately lead to hypoxia and cell death [7, 9].

Oxygen diffusion limitations in tissue or in culture media are usually far more severe than for glucose [10, 11] because even though on a molar basis, oxygen is typically consumed at approximately the same rate as glucose and has a 3–4-fold higher diffusion coefficient than glucose, this is more than offset by the differences in solubility, as oxygen solubility in culture media or in tissue is much lower than that of glucose (e.g., around 0.2 mM vs. 20 mM in aqueous media under atmospheric conditions) [11]. Compared to many other cell cultures or cell transplants, pancreatic islets are particularly susceptible due to their relatively large size, large metabolic demand, and increased sensitivity to hypoxia. In transplanted, non-encapsulated islets, the revascularization process is generally thought to occur over a period of one to two weeks [8, 12]. However, even after revascularization, the number of capillaries found in the transplanted islets seems to be lower than in endogenous islets [12, 13]. Therefore, there is a keen interest to model oxygen consumption in non-vascularized islets and to use the acquired information to improve viability in culture, following transplantation, or under immunoinsulating encapsulation. Various models have already been explored, mainly for immunoisolated islets [10, 14, 15]. Similar models for other, e.g., cardiac tissue have also been explored [16], and they can also be extended to model tissue oxygenation in other cases of interest such as, for example, during pancreas preservation [17] or in cell devices with oxygen permeable silicone membranes [18-20]. However, these studies only incorporated models of diffusive transport.

An important advantage of the present approach is that by exploiting COMSOL Multiphysics' ability to relatively easily couple the convection and diffusion model to Navier–Stokes fluid–mechanics and other application modes, a number of true multiphysics models could be implemented for more complex cases with moving media, e.g., perifusion devices with pump–driven flow or cell cultures with rocking plate–induced agitation. It is hoped that these bring us a few steps closer to truly useful *in silico* physiological models. Computer-based modeling and simulation approaches can be applied in many fields [21-23], but, in general, they can be considered useful [24] only if they can: *(i)* produce predictions or extrapolations that match experimental results; *(ii)* generate data beyond the existing experimental capabilities; *(iii)* enable *in silico* experiments resulting in time–, cost–, and/or effort–savings; *(iv)* reveal non-intuitive mechanistic insights into the working of the system or process; *(v)* identify missing components, processes, or functions in a system; *(vi)* enhance the understanding of visualization of complex processes; and *(vii)* facilitate the consolidation of quantitative data.

2. Governing Equations

Diffusion was assumed to be governed by the generic diffusion equation in its nonconservative formulation (incompressible fluid) [25]:

$$\frac{\partial c}{\partial t} + \nabla \cdot \left(-D\nabla c\right) = R - \mathbf{u} \cdot \nabla c \qquad (1)$$

where, c denotes the concentration [mol·m^{-3}] and D the diffusion coefficient [m^2·s^{-1}] of the species of interest (oxygen), R the reaction rate [mol·m^{-3} ·s^{-1}], $\mathbf{u}$ the velocity field [m·s^{-1}], and ∇ the standard *del* (*nabla*) operator, $\nabla \equiv \mathbf{i}\frac{\partial}{\partial x} + \mathbf{j}\frac{\partial}{\partial y} + \mathbf{k}\frac{\partial}{\partial z}$ [26]. For oxygen consumption, a Michaelis-Menten–type consumption rate ($R < 0$) was assumed as customary in current literature [10, 27]:

$$R_{O_2} = R_{\max,O_2} \frac{c_{O_2}}{c_{O_2} + C_{MM,O_2}} \cdot \delta\left(c_{O_2} > c_{cr}\right) \qquad (2)$$

Accordingly, at very low O_2 concentrations, where cells only try to survive, oxygen consumption scales with the available concentration c_{O_2} and, at sufficiently high concentration, it plateaus at a maximum ($R_{\max}$) (Figure 1). A step–down function δ was also incorporated into the model to account for necrosis (cell death) and eliminate the oxygen consumption of those tissues where c_{O_2} fell below a critical value, c_{crit}, and caused cell death due to hypoxia.

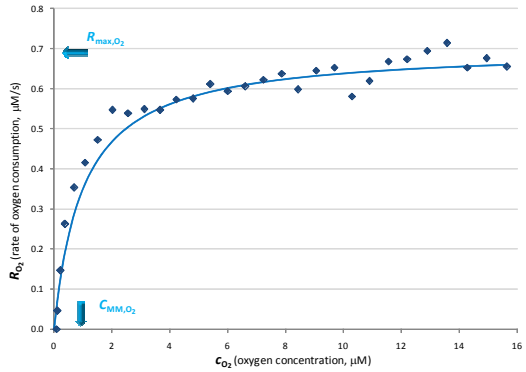

Figure 1. Illustration of Michaelis-Menten–type (rectangular hyperbola–shaped) oxygen consumption using data measured for mitochondria at low oxygen concentrations [27] and fitted with the function of eq. 2 as used here with C_{MM,O_2} of 1 μM.

In the more complex cases where true multiphysics models were needed (§4.3, §4.4), the convection and diffusion model of eq. 1 was coupled to the fluid dynamics, heat transfer, or other models, as needed. For fluid dynamics, the incompressible Navier–Stokes model for Newtonian flow (constant viscosity) was used to calculate the velocity field **u** that results from convection [25, 28]:

$$\rho\frac{\partial \mathbf{u}}{\partial t} - \eta\nabla^2\mathbf{u} + \rho(\mathbf{u}\cdot\nabla)\mathbf{u} + \nabla p = \mathbf{F} \qquad (3)$$

$$\nabla\cdot\mathbf{u} = 0$$

Here, ρ denotes density [kg·m^{-3}], η viscosity [kg·m^{-1}·s^{-1} = Pa·s], p pressure [Pa, N·m^{-2}, kg·m^{-1}·s^{-2}], and **F** volume force [N·m^{-3}, kg·m^{-2}·s^{-2}]. The first equation is the momentum balance; the second one is simply the equation of continuity for incompressible fluids. If required, even more complex models can be built by coupling to other, additional modules. For example, even fluid movement due to thermal expansion-caused buoyancy in the presence of temperature gradients could be incorporated if needed by addition of the heat equation [25]:

$$\rho c_p\frac{\partial T}{\partial t} + \nabla\cdot(-k\nabla T) = Q - \rho c_p\mathbf{u}\cdot\nabla T \qquad (4)$$

Here c_p denotes the heat capacity at constant pressure [J·kg^{-1}·K^{-1}] and k the thermal conductivity [W·m^{-1}·K^{-1}] of the fluid, T the (absolute) temperature [K], and Q the heat source term [W·m^{-3}]. Modeling of moving liquid surfaces, with some limitations, was achieved here by addition of the moving mesh (ALE, arbitrary Lagrangian–Eulerian) module [25], as it was needed for §4.4. In this case, the rocking movement of the fluid was achieved by use of an oscillating gravitational force that has horizontal (F_x) and vertical (F_y) components defined by the inclination angle φ that follows a harmonic oscillation:

$$F_x = \rho g\sin\varphi = \rho g\sin[\varphi_{max}\sin(\omega t)]$$
$$F_y = -\rho g\cos\varphi = -\rho g\cos[\varphi_{max}\sin(\omega t)] \qquad (5)$$

Here, g is the gravitational constant (9.81 m·s^{-2}), φ_{max} the maximum inclination angle, and ω [rad·s^{-1}] the angular frequency (related to the frequency f [Hz] by the usual $\omega = 2\pi f$).

3. Methods

Geometry and meshing. For the present exploratory models, realistic 2D geometries have been used with spherical islets of 100, 150, and 200 μm diameters placed in millimeter-sized device models. COMSOL's predefined 'Extra fine mesh' size was used for meshing resulting in meshes consisting of 5,000–9,000 elements.

Parameter settings. For the present exploratory models, consensus estimates of various parameters available from the literature were used. Oxygen in aqueous solutions obeys Henry's law rather well; i.e., its (mole fraction) solubility (x_{O_2}) is essentially proportional to the partial pressure of oxygen (p_{O_2}) in the surrounding media, $x_{O_2} = p_{O_2}/K_H$ [29]. For the present exploratory calculations, c_{amb} = 0.200 mol·m^{-3} (mM) was assumed for surfaces in contact with atmospheric oxygen. With an oxygen solubility coefficient of α = 1.45×10^{-3} mol·m^{-3}mmHg^{-1} (35°C) [30], this roughly corresponds to a partial pressure p_{O_2} of 140 mmHg. A maximum oxygen consumption rate (per islet) of R_{max} = 0.06×10^{-12} mol/s/islet was used in all calculations. With a standard islet of 150 μm diameter (and islet equivalent IEQ volume V_{IEQ} of 1.77×10^{-12} m^3), this corresponds to a consumption rate (per unit islet volume) of 0.034 mol/s/m^3. This per volume value is similar to that used by Avgoustiniatos and co-workers (0.034 mol/s/m^3 [31]; 0.050 mol/s/m^3 [20]) and Tilakaratne and co-workers (0.046 mol/s/m^3) [14]. As a per islet value, it is similar to that assumed by Dulong and Legallais (0.063×10^{-12} mol/s/islet) [15, 32]; somewhat less than that assumed by Papas, Avgoustiniatos, and co-workers (0.127×10^{-12} mol/s/islet [17, 18];

0.074×10^{-12} mol/s/islet [33]); and slightly larger than those measured recently in various settings by Sweet and co-workers (e.g., 0.025–0.048×10^{-12} mol/s/islet at 3 mM basal- or 20 mM high glucose [34, 35]). As Michaelis–Menten constant, $C_{MM,O_2} = 1.0\times10^{-3}$ mol/m^3 (1 μM) was assumed, corresponding to $p_{MM,O_2} = 0.7$ mmHg – similar to the frequently used 0.44 mmHg value [10, 14, 17, 20] or even to that determined originally for mitochondria [27]. A step–down function, δ, was also added to account for necrosis and cut the oxygen consumption when the concentration falls below a critical value, $c_{crit} = 1.0\times10^{-4}$ mol/m^3 (corresponding to $p_{cr,O_2} = 0.07$ mmHg; comparable with the commonly used 0.10 mmHg [10, 17, 20]). To avoid computational problems, Comsol's smoothed Heaviside function with a continuous first derivative and without overshoot `flc1hs` [36] was used as step-down function, $\delta(c)$ = flc1hs(c – 0.0001, 0.00005).

For the diffusion coefficient of oxygen in aqueous media, $D_{O_2,w} = 3.0\times10^{-9}$ m^2·s^{-1} was assumed as a reasonable approximation for O_2 diffusion in water at 37°C considering the commonly accepted value of 2.4×10^{-9} m^2·s^{-1} at 25°C [30] and a measured value of 3.1×10^{-9} m^2·s^{-1} at 45°C or fitted diffusivity equations such as the Wilke-Chang or Othmer-Thakar estimates for diffusion coefficient in aqueous solutions [37]. For the diffusion coefficient of oxygen in tissue, $D_{O_2,t} = 2.0\times10^{-9}$ m^2·s^{-1}, was assumed; slightly less than in water and the same value that was used by Radisic, Vunjak-Novakovic and co-workers [16]. Avgoustiniatos and co-workers have recently determined a somewhat lower value for the effective diffusion coefficient of oxygen in rat pancreatic islets (1.3×10^{-9} m^2·s^{-1}) [31]. The same value was used for the diffusion coefficient in silicone being similar to measured values [38, 39]. For cases where convective flow was also allowed in the model, an essentially aqueous media at body temperature was assumed as a first estimate (e.g., $T_0 = 310.15$ K, $\rho = 993$ kg·m^{-3}, $\eta = 0.7\times10^{-3}$ Pa·s, $c_p = 4200$ J·kg^{-1}K^{-1}, $k_c = 0.634$ J·s^{-1}m^{-1}K^{-1}, $\alpha = 2.1\times10^{-4}$ K^{-1}).

Boundary conditions. In the convection and diffusion models, the following conditions were used: insulation/symmetry, $\mathbf{n}\cdot(-D\nabla c+c\mathbf{u}) = 0$, for walls, continuity for islets, and fixed concentration ($c = c_{amb}$) for liquid surfaces in contact with exterior media. For the case of diffusion through a membrane (§4.2), a membrane/media partition coefficient $K_p = c_{membr}/c$ was built into the model for oxygen through a special boundary condition using the stiff-spring method [40]. An additional, separate concentration variable c_2 was added for the membrane (with a corresponding application mode), and to maintain continuous flux at the interface, an inward flux boundary condition was imposed along the membrane-fluid boundary with $\upsilon(c_2 - K_p c)$ and υ = 10,000 m·s^{-1}. In the incompressible Navier-Stokes models, no slip ($\mathbf{u} = 0$) was used along all surfaces corresponding to liquid-solid interfaces (except those in the rocking plate models, where slip was also explored due to convergence problems). For the perifusion chamber (§4.3), a parabolic inflow velocity profile, $4v_{in}(y/y_{max})(1–y/y_{max})$, was used on the inlet and pressure, no viscous stress with $p_0 = 0$ on the outlet. In the moving mesh (ALE) model (§4.4), no mesh displacement was allowed on the bottom and the islets (dx, dy = 0), no horizontal displacement on the walls (dx = 0), and a normal mesh velocity of $\mathbf{u}\cdot\mathbf{n}$ (u·nx+u·ny) was imposed on the top boundary.

Postprocessing and visualization. Surface plots with a preset range (0.0001–0.200 mol·m^{-3}) were used for c_{O_2} and arrows for the oxygen flux. For the case of the two-concentration membrane model (§4.2), a c_{all} was defined using subdomain expressions to visualize the two different concentrations in the same graph. For §4.3 and §4.4, arrows and streamlines for the velocity field were also used. For the rocking culture device (§4.4), inclination of the device was visualized by using the 'Deformed shape plot' function with X and Y components synchronized to the oscillation of the gravitational field ($y\cdot\sin\varphi$ and $–x\cdot\sin\varphi$, respectively) both for the sub-domain and boundary data as described in [41]. Animations were generated with the same settings used for the corresponding graphs.

Implementation. All models were implemented in Comsol Multiphysics 3.4 and solved as time-dependent problems up to sufficiently long final times to reach steady state allowing free or intermediate time-steps for the solver. Computations were done with the UMFPACK direct solver as linear system solver on a Dell Precision 690 PC with a 3.2 GHz CPU running Linux.

4. Results and Discussion

4.1. Standard culture

The oxygen distribution obtained with a fully scaled 2D cross section of three differently sized islets in a traditional culture model is shown in Figure 2.

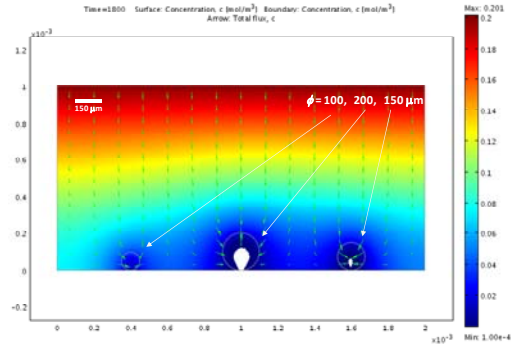

Figure 2. Calculated oxygen concentration for three islets (with diameters ϕ = 100, 150, and 200 µm) in standard culture conditions after stationary conditions have been reached (h = 1 mm assumed). The color-coded surface represent the oxygen concentration (red corresponding to higher and blue to lower values), whereas green arrows represent oxygen flux. Areas with values below a critical value ($<10^{-4}$ mol·m^{-3}), where the lack of oxygen (hypoxia) is predicted to cause cell death (necrosis) are left uncolored (white).

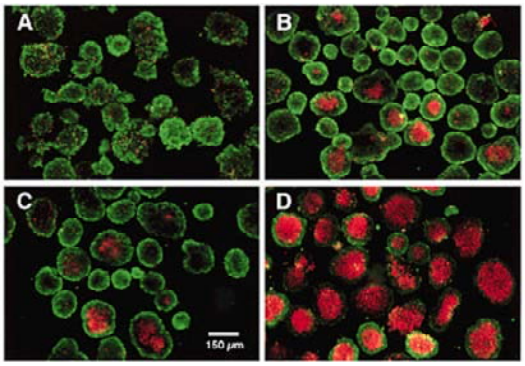

Figure 3. Viability of isolated rat islets with green fluorescence corresponding to live- and red to dead cells (determined using Calcein-AM and propidium iodide viability stains). **A**: freshly isolated, **B**: 24 h normoxic culture (95% air, 5% CO_2), **C**: 48 h normoxic culture, **D**: 24 h normoxic followed by 24 h hypoxic (1% O_2) culture. Copyright © 1998 American Diabetes Association from [7]. Reprinted with permission from The American Diabetes Association.

These results are in good agreement with various experimental observations (Figure 3) indicating that when isolated islets are cultured for 24–48 h in normoxic culture conditions, large islets show central necrosis, which becomes much more severe after exposure to hypoxic culture conditions [7]. As a first estimate, even the size of the necrotic core as measured for rat islets in [7] or [42] is well predicted suggesting that these exploratory models might already provide reasonable quantitative estimates and not just qualitative fit. It should be noted that in all these models, instantaneous death for tissues was assumed as soon as the local c_{O_2} values fell below the critical threshold. Hence, while the models are ultimately realistic, the time-scales are probably not since under critical conditions, real islets and cells can probably shut down their metabolism and linger around for some time before irreversible death occurs.

Obviously oxygenation can be improved by lowering the density of the consuming tissue, by reducing the diffusion path in the media, or by increasing the outside oxygen concentration. For example, at a lower cell density, a single standard islet (ϕ = 150 µm) can survive in the same culture as Figure 2 without necrosis of its core (Figure 4). Since these are 2D cross-sections, Figure 2 roughly corresponds to a 3D culture density of about 1,600 IEQ/cm^2.

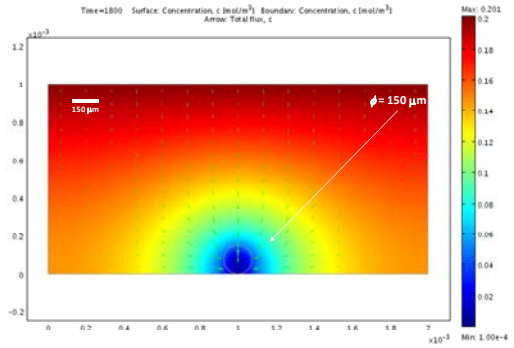

Figure 4. Calculated oxygen concentration for a single (ϕ = 150 µm) islet for the same conditions of Figure 2.

Because of these hypoxia-related problems, current islet culture techniques require low surface coverage, and, hence, up to 30 or more flasks per human pancreas (i.e., ~20,000–30,000 IEQ in 30 mL of medium per flask corresponding to 100–200 IEQ/cm^2 and a flask surface utilization of only 2–3%) [18, 43]. This is a considerable hindrance both for research settings and for clinical applications. Consequently, various attempts are being made to enhance oxygenation, for example, by use of

silicone rubber membranes [18-20] due to their high oxygen-permeability [38] or by use of bioreactors with rocking plates and wave-induced agitation [44, 45]. Exploratory computational models for some of these are presented in the following subsections.

4.2. Oxygen-permeable membrane bottoms

Use of cell culture devices with oxygen-permeable membrane bottoms is a promising alternative being explored to ensure better oxygenation [18, 19]. Silicone rubber-based membranes are a preferred choice due to their high oxygen-permeability [38].

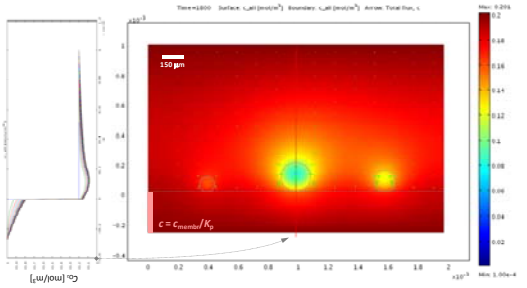

Figure 5. Calculated oxygen concentration for the three islets of Figure 2 for the same conditions, but with a device with an oxygen-permeable bottom membrane. Concentrations in the membrane are higher than in the media as shown on the rotated figure on the left, which illustrates c_{O_2} along the middle cross section together with its progression in time, but were rescaled using the partition coefficient $K_p = c_{membr}/c$ for the color-coded surface plot.

With such membranes, much better oxygenations can be achieved even at higher cell densities [18-20], and the 'oxygen sandwich' designation [19] is justified as O_2 can reach the islets from both sides with a much larger flux coming through the membrane. It should be noted that because in such membranes CO_2 tends to have an even higher permeability than O_2 [38], in certain cases, it might reach undesirably elevated or undesirably low levels (depending on the outside concentrations).

4.3. Perifusion device with flow

Perifusion studies are now routinely used to assess islet quality and function as they allow the dynamic measurement of the glucose-stimulated insulin release (GSIR) [46-49] through the continuous monitoring of the insulin (and/or other metabolic products) released by islets placed in a perifusion column and exposed to varying levels of incoming glucose solutions. The present multiphysics approach allows not only modeling of the oxygen concentration in the islets and the flowing media, but even its adjustment to account for the increase in oxygen consumption with the increase in glucose concentration due to increased metabolic demand [47, 50] by making R_{max,O_2} in eq. 2 a function of c_{gluc} as illustrated by Figure 6 below.

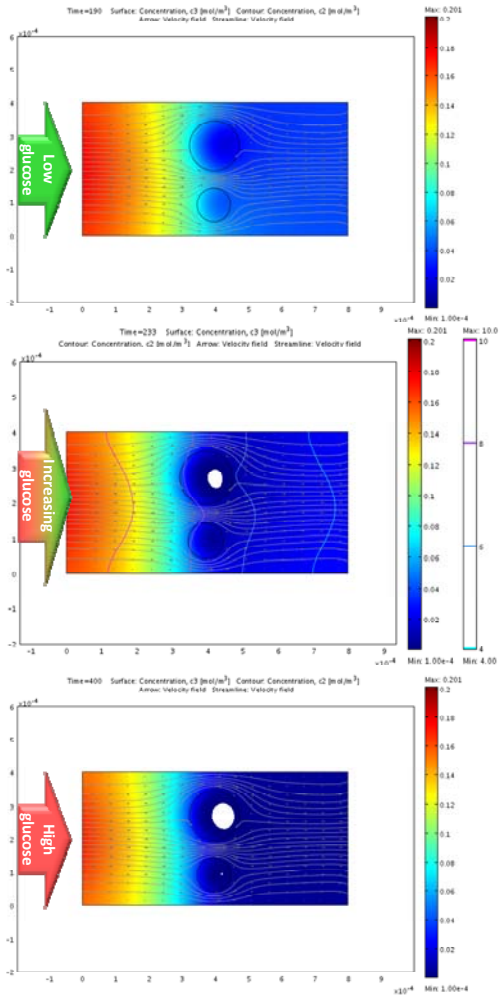

Figure 6. Oxygen levels in a perifusion chamber model with two islets at steady state conditions corresponding to low (3 mM) and high (11 mM) glucose concentrations (top and bottom, respectively; media flows from left to right at constant flux). The velocity field (gray arrows) and the streamlines corresponding to the flow of the perifusion media are also shown (see Figure 7 for another illustration of the velocity field). The central image depicts a time-point during the transition from low to high incoming glucose as highlighted by the corresponding contour lines of the glucose gradient.

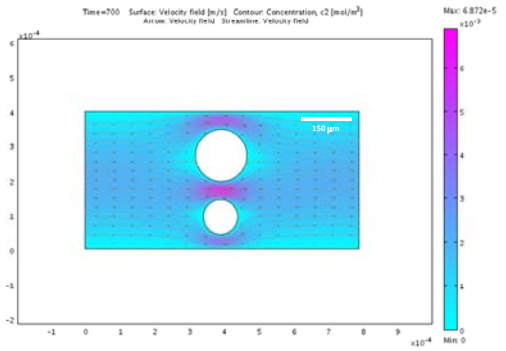

Figure 7. The velocity field of the fluid flow for the same configuration of Figure 6 depicted by a color-coded surface, proportional arrows, and streamlines.

4.4. Rocking plate–induced agitation

Devices with rocking plates and wave-induced agitation [44, 45] are also being explored as a possible approach to ensure better oxygenation. For example, the Wave Bioreactor™ system, which is currently marketed by GE Healthcare, is one such alternative. Results obtained here with a draft model for a small rocking plate with a maximum inclination angle, φ_{max}, of 1° and a rocking frequency of 0.08 Hz (5 min^{-1}) are shown in Figure 8; they indicate only a small improvement over §4.1, i.e., the percent area of necrotic tissue in the core of larger islets decreased, but only by a few percents. It has to be noted, however, that this can be considered only a draft, exploratory model since it does not account for surface tension effects and convergence could be consistently achieved only by allowing slip along all fluid-solid boundaries; therefore, unrealistically high viscosity (similar to that of glycerol) had to be assumed for the media to avoid very large movements of the liquid.

5. Conclusion

In conclusion, various exploratory cellular–level models for the oxygen consumption of nonvascularized pancreatic islets with physiologically relevant geometries have been implemented in COMSOL Multiphysics. Results are in good agreement with existing experimental evidence, and the corresponding animations obtained here provide graphical illustrations for the progress of necrosis within the inner cores of larger islets when oxygen availability is limited. The present exploratory calculations can be relatively easily extended to various other geometries, and such *in silico* models should be particularly useful (*i*) to improve the design of cell culture and cell transplant (i.e., bioartificial pancreas) devices, (*ii*) to increase the viability and functionality of isolated pancreatic islets, which is of crucial clinical relevance for islet transplantation, and (*iii*) to clarify the processes leading to hypoxia-induced necrosis in nonvascularized tissues.

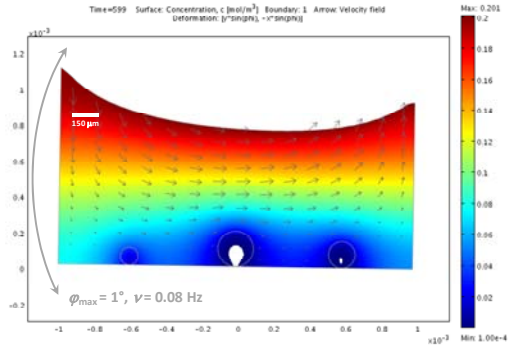

Figure 8. Calculated oxygen concentration for the three islets of Figure 2 for the same conditions, but with a device with rocking plate–induced agitation. Gray arrows represent the velocity field of the media movement due to the wave-generating rocking plate.

6. References

1. Ricordi, C.; Strom, T. B. Clinical islet transplantation: advances and immunological challenges. *Nat. Rev. Immunol.,* **4**, 259-268 (2004).

2. Shapiro, A. M.; Lakey, J. R.; Ryan, E. A.*, et al.* Islet transplantation in seven patients with type 1 diabetes mellitus using a glucocorticoid-free immunosuppressive regimen. *N. Engl. J. Med.,* **343**, 230-238 (2000).

3. Konstantinova, I.; Lammert, E. Microvascular development: learning from pancreatic islets. *Bioessays,* **26**, 1069-1075 (2004).

4. Cabrera, O.; Berman, D. M.; Kenyon, N. S.*, et al.* The unique cytoarchitecture of human pancreatic islets has implications for islet cell function. *Proc. Natl. Acad. Sci. USA,* **103**, 2334-2339 (2006).

5. Suckale, J.; Solimena, M. Pancreas islets in metabolic signaling - focus on the beta-cell. *Front. Biosci.,* **13**, 7156-7171 (2008).

6. Lifson, N.; Lassa, C. V.; Dixit, P. K. Relation between blood flow and morphology in islet organ of rat pancreas. *Am. J. Physiol. Endocrinol. Metab.,* **249**, E43-E48 (1985).

7. Vasir, B.; Aiello, L. P.; Yoon, K. H.*, et al.* Hypoxia induces vascular endothelial growth factor gene and protein expression in cultured rat islet cells. *Diabetes,* **47**, 1894-1903 (1998).

8. Jansson, L.; Carlsson, P. O. Graft vascular function after transplantation of pancreatic islets. *Diabetologia,* **45**, 749-763 (2002).

9. Narang, A. S.; Mahato, R. I. Biological and biomaterial approaches for improved islet transplantation. *Pharmacol. Rev.,* **58**, 194-243 (2006).

10. Avgoustiniatos, E. S.; Colton, C. K. Effect of external oxygen mass transfer resistances on viability of immunoisolated tissue. *Ann. N.Y. Acad. Sci.,* **831**, 145-167 (1997).

11. Martin, Y.; Vermette, P. Bioreactors for tissue mass culture: design, characterization, and recent advances. *Biomaterials,* **26**, 7481-7503 (2005).

12. Carlsson, P. O.; Mattsson, G. Oxygen tension and blood flow in relation to revascularization in transplanted adult and fetal rat pancreatic islets. *Cell Transplant.,* **11**, 813-820 (2002).

13. Carlsson, P. O.; Palm, F.; Andersson, A.*, et al.* Chronically decreased oxygen tension in rat pancreatic islets transplanted under the kidney capsule. *Transplantation,* **69**, 761-766 (2000).

14. Tilakaratne, H. K.; Hunter, S. K.; Rodgers, V. G. Mathematical modeling of myoglobin facilitated transport of oxygen in devices containing myoglobin-expressing cells. *Math. Biosci.,* **176**, 253-267 (2002).

15. Dulong, J. L.; Legallais, C. A theoretical study of oxygen transfer including cell necrosis for the design of a bioartificial pancreas. *Biotechnol. Bioeng.,* **96**, 990-998 (2007).

16. Radisic, M.; Deen, W.; Langer, R.*, et al.* Mathematical model of oxygen distribution in engineered cardiac tissue with parallel channel array perfused with culture medium containing oxygen carriers. *Am. J. Physiol. Heart Circ. Physiol.,* **288**, H1278-H1289 (2005).

17. Papas, K. K.; Hering, B. J.; Gunther, L.*, et al.* Pancreas oxygenation is limited during preservation with the two-layer method. *Transplant. Proc.,* **37**, 3501-3504 (2005).

18. Papas, K. K.; Avgoustiniatos, E. S.; Tempelman, L. A.*, et al.* High-density culture of human islets on top of silicone rubber membranes. *Transplant. Proc.,* **37**, 3412-3414 (2005).

19. Fraker, C. A.; Alvarez, S.; Papadopoulos, P.*, et al.* Enhanced oxygenation promotes beta cell differentiation in vitro. *Stem Cells,* **25**, 3155-3164 (2007).

20. Avgoustiniatos, E. S.; Hering, B. J.; Rozak, P. R.*, et al.* Commercially available gas-permeable cell culture bags may not prevent anoxia in cultured or shipped islets. *Transplant. Proc.,* **40**, 395-400 (2008).

21. Buchwald, P.; Bodor, N. Computer-aided drug design: the role of quantitative structure-property, structure-activity, and structure-metabolism relationships (QSPR, QSAR, QSMR). *Drugs Future,* **27**, 577-588 (2002).

22. Buchwald, P. A general bilinear model to describe growth or decline time-profiles. *Math. Biosci.,* **205**, 108-136 (2007).

23. Fall, C. P.; Marland, E. S.; Wagner, J. M.*, et al.* Computational Cell Biology; Springer-Verlag: New York, pp 468 (2002).

24. Materi, W.; Wishart, D. S. Computational systems biology in drug discovery and development: methods and applications. *Drug Discov. Today,* **12**, 295-303 (2007).

25. Comsol, AB *COMSOL Multiphysics Modeling Guide, version 3.4*, COMSOL AB (2007).

26. Riley, K. F.; Hobson, M. P.; Bence, S. J. *Mathematical Methods for Physics and Engineering. A Comprehensive Guide*, Cambridge University Press, Cambridge (1997).

27. Wilson, D. F.; Rumsey, W. L.; Green, T. J.*, et al.* The oxygen dependence of mitochondrial oxidative phosphorylation measured by a new optical method for measuring oxygen concentration. *J. Biol. Chem.,* **263**, 2712-2718 (1988).

28. Bocca, N.; Ricordi, C.; Kenyon, N. S.*, et al.* 3-D Multiphysics FEM modeling to optimize local drug delivery in a biohybrid device designed for cell transplant. In *Proceedings of the Comsol Conference 2007 Boston*; Dravid, V., Ed.; Comsol, Inc., Boston pp. 101-107 (2007).

29. Silbey, R. J.; Alberty, R. A.; Bawendi, M. G. *Physical Chemistry*, 4th ed., Wiley, New York (2005).

30. Lide, D. R., (Ed.) *CRC Handbook of Chemistry and Physics*, 87th ed., CRC Press, Boca Raton (2006-2007).

31. Avgoustiniatos, E.; Dionne, K. E.; Wilson, D. F.*, et al.* Measurements of the effective diffusion coefficient of oxygen in pancreatic islets. *Ind. Eng. Chem. Res.,* **46**, 6157-6163 (2007).

32. Dulong, J. L.; Legallais, C. Contributions of a finite element model for the geometric optimization of an implantable bioartificial pancreas. *Artif. Organs,* **26**, 583-589 (2002).

33. Papas, K. K.; Pisania, A.; Wu, H.*, et al.* A stirred microchamber for oxygen consumption rate measurements with pancreatic islets. *Biotechnol. Bioeng.,* **98**, 1071-1082 (2007).

34. Sweet, I. R.; Gilbert, M.; Jensen, R.*, et al.* Glucose stimulation of cytochrome C reduction and oxygen consumption as assessment of human islet quality. *Transplantation,* **80**, 1003-1011 (2005).

35. Sweet, I. R.; Gilbert, M.; Scott, S.*, et al.* Glucose-stimulated increment in oxygen consumption rate as a standardized test of human islet quality. *Am. J. Transplant.,* **8**, 183-192 (2008).

36. Comsol, AB *COMSOL Multiphysics User's Guide, version 3.4*, COMSOL AB (2007).

37. Hayduk, W.; Laudie, H. Prediction of diffusion coefficients for nonelectrolytes in dilute aqueous solutions. *AIChE J.,* **20**, 611-615 (1974).

38. Robb, W. L. Thin silicone membranes-their permeation properties and some applications. *Ann. NY Acad. Sci.,* **146**, 119–137 (1968).

39. Jenkins, D. M.; Krishnan, A. Surface limitations for gas transport through a silicone film. *ASAE/CSAE Meeting Paper*, Number: 043052 (2004).

40. Comsol, AB *COMSOL Multiphysics Chemical Engineering Module Model Library, version 3.4*, COMSOL AB (2007).

41. Comsol, AB *COMSOL Multiphysics Model Library, version 3.4*, COMSOL AB (2007).

42. MacGregor, R. R.; Williams, S. J.; Tong, P. Y.*, et al.* Small rat islets are superior to large islets in in vitro function and in transplantation outcomes. *Am. J. Physiol. Endocrinol. Metab.,* **290**, E771-E779 (2006).

43. Ichii, H.; Pileggi, A.; Khan, A.*, et al.* Culture and transportation of human islets between centers In *Islet Transplantation and Beta Cell Replacement Therapy*; Shapiro, A. M. J., Shaw, J. A. M., Eds.; Informa Healthcare New York pp. 251-268 (2007).

44. Singh, V. Disposable bioreactor for cell culture using wave-induced agitation. *Cytotechnology,* **30**, 149-158 (1999).

45. Mikola, M.; Seto, J.; Amanullah, A. Evaluation of a novel Wave Bioreactor® cellbag for aerobic yeast cultivation. *Bioprocess. Biosyst. Eng.,* **30**, 231–241 (2007).

46. Dionne, K. E.; Colton, C. K.; Yarmush, M. L. Effect of hypoxia on insulin secretion by isolated rat and canine islets of Langerhans. *Diabetes,* **42**, 12-21 (1993).

47. Sweet, I. R.; Khalil, G.; Wallen, A. R.*, et al.* Continuous measurement of oxygen consumption by pancreatic islets. *Diabetes Technol. Therap.,* **4**, 661-672 (2002).

48. Bocca, N.; Pileggi, A.; Molano, R. D.*, et al.* Soft corticosteroids for local immunosuppression: exploring the possibility for the use of loteprednol etabonate in islet transplantation. *Pharmazie,* **63**, 226-232 (2008).

49. Cabrera, O.; Jacques-Silva, M. C.; Berman, D. M.*, et al.* Automated, high-throughput assays for evaluation of human pancreatic islet function. *Cell. Transplant.,* **16**, 1039-1048 (2008).

50. Wang, W.; Upshaw, L.; Strong, D. M.*, et al.* Increased oxygen consumption rates in response to high glucose detected by a novel oxygen biosensor system in non-human primate and human islets. *J. Endocrinol.,* **185**, 445-455 (2005).

7. Acknowledgements

The financial support of the Diabetes Research Foundation (www.diabetesresearch.org) that made this work possible is gratefully acknowledged.